JOURNAL OF Applied Polymer SCIENCE

# Enhancing Particle Erosion Resistance of Glass-Reinforced Polymeric Composites Using Carbon Nanofiber-Based Nanopaper Coatings

**Na Zhang,[1,2] Fan Yang,[1*] Dante Guerra,[3] Changyu Shen,[2] Jose Castro,[3] James Ly Lee[1]**

[1]Department of Chemical and Biomolecular Engineering, The Ohio State University, Columbus, Ohio 43202

[2]Department of Materials Science and Engineering, Zhengzhou University, Zhengzhou 450052, China

[3]Department of Integrated Systems Engineering, The Ohio State University, Columbus, Ohio 43202

*Present address: Department of Mechanical and Industrial Engineering, University of Toronto, Toronto, ON M5S 3G8, Canada

N. Zhang and F. Yang are contributed equally to this work.

Correspondence to: J. L. Lee (E-mail: lee.31@osu.edu)

**ABSTRACT:** Sand erosion may cause severe damage of blades in wind turbine and helicopter blades as well as many surface components of airplanes. In this study, thin nanopapers made of carbon nanofibers (CNFs) are used to enhance the resistance of solid particle erosion of glass fiber (GF)/wind epoxy composites. Finite element computer simulations are used to elucidate the underlying mechanisms. The much higher particle erosion resistance of nanopapers compared to GF-reinforced epoxy composites is attributed to the high strength of CNFs and their nanoscale structure. The excellent performance in particle erosion resistance makes the CNF-based nanopaper a prospective protective coating material for the turbine blades in the wind energy industry. © 2012 Wiley Periodicals, Inc. J. Appl. Polym. Sci. 129: 1875–1881, 2013

**KEYWORDS:** composites; mechanical properties; fibers; coatings; structure–property relations

Received 3 October 2012; accepted 30 November 2012; published online 24 December 2012

**DOI: 10.1002/app.38899**

## INTRODUCTION

One of the most attractive environmentally friendly energy sources is wind power. It has been the world's fastest growing renewable energy source for more than a decade with an average annual growth rate of over 20%. In 2008, the United States had a record breaking year by increasing the wind energy generating capacity by 50%.[1] An important issue in the wind energy industry is the erosive wear of leading edges of turbine blades by particulate-laden winds, which can significantly debase the turbine performance.[2–6] Surface engineering is an effective way to mitigate the erosion. Among various coating materials, thermoplastic polyurethane (TPU) is the most widely used one due to its excellent erosive-resistance behavior.[2] However, the TPU coating needs to be adequately thick (~ 1 mm) to provide effective protection, causing a change of the blade aerodynamic profile and as a consequence, reduced power production efficiency.[2] The overall strength and rigidity of the turbine blades are also compromised by the relative weak coating materials.

Fiber-reinforced polymers (FRPs), such as glass fiber (GF)-reinforced epoxy, possess excellent properties such as high modulus-to-weight ratio and high strength-to-weight ratio,[7,8] making them widely used as structural materials in the aerospace, transportation, and energy production industries. The erosion performance of FRP materials has also attracted much attention.[3–5,9,10] In the literature, some authors reported that the erosion rate of conventional FRP was larger than that of the neat resin,[10–12] whereas others reported the opposite.[10] The inconsistency in the experimental results may be attributed to differences in the configuration of the microstructure and the strength of the fiber–matrix interface.[10,13,14] Nevertheless, the performance of available FRPs is disappointing with respect to particle erosion resistance when compared to metallic materials and elastomers, and needs improvement. Some efforts have been made to utilize nanoparticles to enhance the erosion resistance of FRPs. Balani et al.[15] studied the wear resistance of $Al_2O_3$–carbon nanotube (CNT) nanocomposites at different length scales. Bao et al.[16] studied the particle erosion behavior of the vapor-grown carbon fiber reinforced unsaturated polyester resin composites. Liang et al.[17] investigated multifunctional properties such as the vibration damping, hydrophobicity, and the impact-friction resistance for CNF-based nanocomposite coatings.

In this study, we investigated the use of a thin protective layer of CNF nanopaper for improving the erosive resistance of composites. A series of sand erosion experiments were carried out on GF/wind epoxy composites with and without CNF

Applied Polymer SCIENCE

nanopaper surface layer to compare their performance in particle erosion. Computer simulations of the FE method were used to explain the underlying mechanisms and to investigate the effects of coating thickness and CNF content of nanopapers. We show that when the microstructure dimensions of the composites decreased to the nanometer scale and the GF was replaced by the stronger CNF on the composite surface, the erosion resistance of the material was greatly improved.

## EXPERIMENTAL

The CNF used in this study was a vapor-grown carbon nanofiber, Pyrograf®-III (PR-24-XT-HHT), obtained from Applied Sciences (Cedarville, OH). The length of CNFs is about 30–100 $\mu$m, and the average diameter is 0.1 $\mu$m. A stitched unidirectional GF mat, QM6408 from Brunswick Technologies (Brunswick, ME), was used as the long fiber reinforcement. The epoxy resin used was EPIKOTETM RIM 135 with an epoxy equivalent weight of about 166–185, and a diamine curing agent, EPIKURETM RIM H 137 with an amine value of about 400–600 mg [KOH]/g, provided by Hexion Specialty Chemicals (Houston, TX). This is a low-temperature and low-viscosity resin designed especially for manufacturing wind turbine blades. Blocky, sharp edged green $SiO_2$ particles with a size about 150 $\mu$m and a hardness of 2600 Knoop were selected as the erodents.

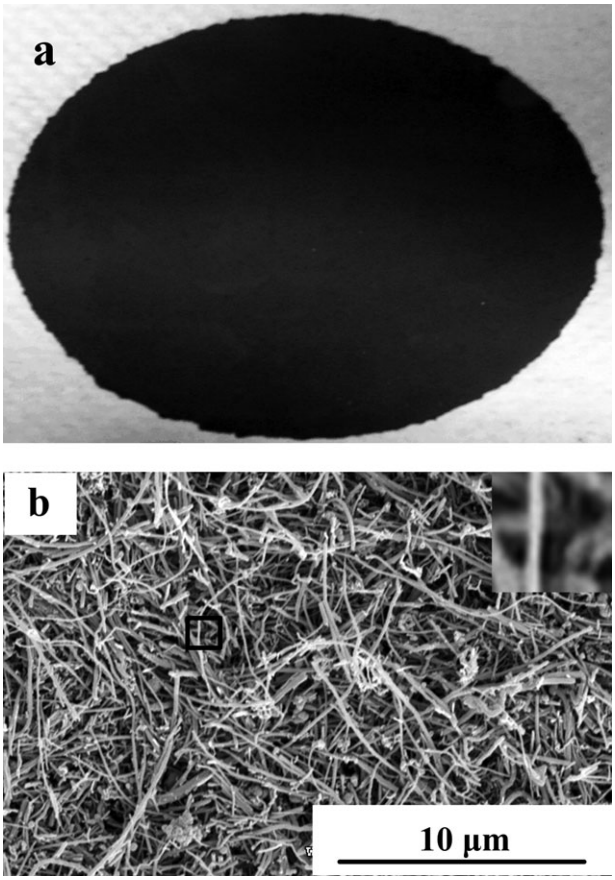


**Figure 1.** (a) CNF nanopaper and (b) SEM picture of CNF paper, the upper right inset is an enlarged view of the 1 × 1 $\mu m^2$ region indicated by the square.

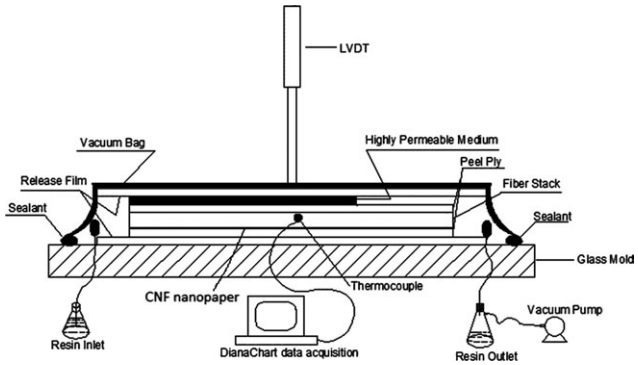


**Figure 2.** Schematic of the VARTM setup.

The nanopapers were prepared using vacuum filtration. The setup used consisted of a 90-mm diameter glass filter holder with a stainless steel screen membrane support placed over a conical flask. A hydrophilic polycarbonate membrane filter with a pore size of 0.4 $\mu$m (Millipore) was placed flat in the setup and clamped. It was connected to a vacuum aspirator pump. The nanoparticle solution was prepared as follows: the CNF particles were redispersed in deionized water and sonicated using a Branson Digital Sonifier [(S450D), 75% amplitude, from Newtown, CT] for 30 min. The resulting suspension was cooled down for 30 min in a refrigerator and sonicated again for 30 s and then, filtered with the filtration setup previously described under a pressure of $\sim$ 400 kPa. Vacuum was applied for about 20 min after all the water was filtered. The CNF nanopapers were dried overnight at room temperature. A typical resulting CNF nanopaper and its scanning electron microscopy (SEM) picture are shown in Figure 1(a,b), respectively. From Figure 1(b), we can observe that the diameter of the CNF is about 100 nm.

Vacuum-assisted resin transfer molding (VARTM) shown schematically in Figure 2 was used to impregnate the GF and GF/CNF nanopaper preforms. A preform consisting of five layers of GF mats and one layer of CNF nanopaper was sealed with a vacuum bag. Before mold filling, vacuum was applied to force the bag to press tightly against the fiber stack. The epoxy mixture was degassed in a vacuum chamber for 15 min before the resin was infused into the fiber preforms. The samples were cured at room temperature ($\sim$ 20°C) for 24 h and postcured at 80°C for an additional 15 h. The GF and CNF content in the composites were controlled at 65 and 2.5 wt %, respectively.

For erosion wear resistance, materials can be classified into ductile and brittle categories according to their behavior with respect to the impinging angle and erosion process.[10] In brittle erosion, the weight loss increases linearly with time, whereas in a ductile type the particles may be embedded in the target surface causing a weight gain initially, followed with a linear weight loss as a function of time by further impingement. The maximum weight loss is found at about 90 and 30° impact angles for brittle and ductile erosions, respectively.[10] As both GF/CNF nanopaper/epoxy and GF/epoxy showed brittle erosion mode with the maximum erosion rate at normal impinge, the impinge angle was chosen as 90° in this study.

All the erosion tests were performed at room temperature in a sand-blasting chamber equipped with a boron carbide jet nozzle with an internal diameter of 8 mm. The distance between the sample holder and the nozzle was 7.6 cm for all experiments. The impact angle was adjusted by turning the sample holder. The air pressure in the nozzle was kept constant at 0.4 MPa. The eroded area was also constant, as a steel cover frame with a rectangular opening was placed on the surface of the test specimens. The composite weight loss was measured by a precision balance (Explorer, EP214C, Pine Brook, NJ). Before weighing, the $SiO_2$ particles were removed from the sample surface by air blasting and cleaned with acetone. The erosive wear behavior was characterized through the weight loss of the samples. The eroded surface texture was measured with a Mitutoyo contact profilometer (Mitutoyo America, S-3000, Aurora, IL). SEM images were collected using a field emission scanning electron microscope, Hitachi S-4300 (Tokyo, Japan). The samples were gold sprayed to reduce charging of the surface.

## FINITE ELEMENT SIMULATION

To elucidate the mechanisms of particle erosion, finite element (FE) simulations were carried out for GF/epoxy composites with and without CNF nanopaper coating. In contrast to the experiments that involved a large number of collision events, only one collision event was simulated to qualitatively depict the effect of various parameters in FE analysis.[18–20] The configuration of particle erosion on the surface of a GF/epoxy composite is shown in Figure 3(a), whereas Figure 3(b) shows the representative volume elements (RVEs) for computation for both GF/epoxy composites and CNF nanopaper. The right graph in Figure 3(b) shows an enlarged view of a small portion of the fiber skeleton in the CNF nanopaper model. Qualitative comparisons were made between the experiments and the simulations to elucidate the particle erosion mechanisms.

The simulations were carried out using the generalized FE codes ABAQUS/EXPLICIT version 6.9. Three-dimensional computational RVEs were generated, and one collision event with periodically distributed particles was simulated. As the impinge angle was chosen as 90°, only one-fourth of the particle-target periodic configuration was needed in the RVEs utilizing periodicity and symmetry. Based on the experimental situations, the diameter of the spherical eroding particle was chosen as 0.2 mm, and the distance between the centers of two adjacent particles was 0.4 mm. Thus, the lateral dimension $L_x$, $L_y$ in Figure 3(b) is 0.2 mm. The GF fibers had a diameter of 120 $\mu$m, and their interspaces along the lateral and thickness directions were 0.28 and 0.15 mm, respectively. The thickness $L_z$ changed with the number of stacked GF layers, that is, a thickness of 0.3 mm corresponds to two GF layers, and a thickness of 0.45 mm corresponds to three GF layers. For the nanopaper, the construction of the random fabric in Figure 1(b) would cause huge difficulty to the mesh of the simulation. Instead, CNFs were interwoven into a uniform orthogonal beam framework to represent the highly interlaced microstructure of nanopaper. It can be noted that a large number of elements and hence much computation expense were needed due to the huge difference between the CNF diameter and the dimension of simulation

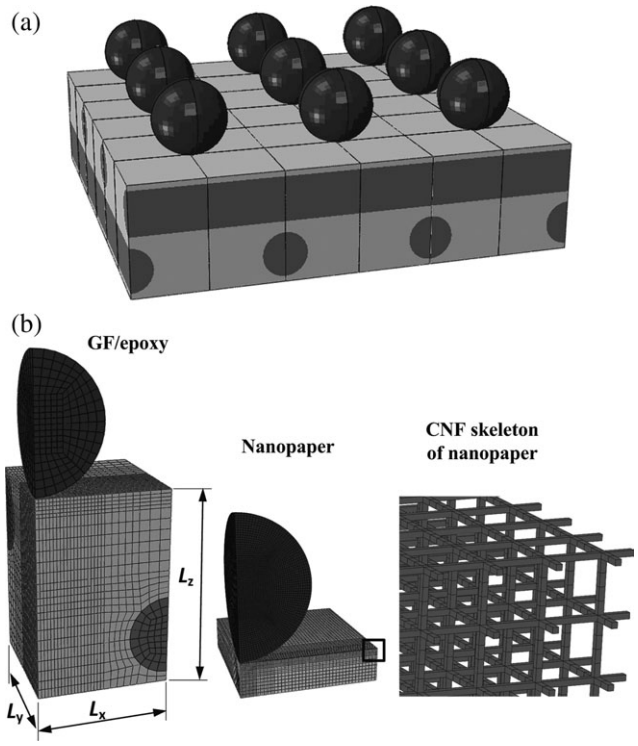


**Figure 3.** FE simulation models. (a) Configuration of the particle erosion on surface of GF/epoxy composite and (b) Computational RVEs for GF/epoxy composites and nanopaper. The right graph shows the enlarged view of the skeleton of CNFs in nanopaper of the portion indicated by the square.

RVE, which was dependent on the size of the impinging particle. The thinner CNF leaded to larger computational expense. In this work, the fiber diameter of CNF was chosen as 0.5 $\mu$m, which was larger than in the experiments to save computational expense. And the fiber interspace was chosen as 5 $\mu$m. Despite this, the obtained model contained 338,428 elements, corresponding to more than 100 CPU hours for a typical run on a 2.6 GHz dual core computer for 0.5 ms of simulation time.

Symmetric boundary conditions were applied on the nodes on the four lateral faces of the nanopaper and GF/epoxy composite models, as well as on the cross-section faces of the erodent particles. For all models, the nodes on the bottom faces were constrained using fixed boundary conditions. The particles were initially located at a small distance above the surface with an initial velocity of 10 m/s, which is smaller than the experimental situation (around 50 m/s) to avoid excessive over-closure of contact surfaces during the simulation that may cause computational failure.

The linear eight-node element C3D8 was used for modeling the eroding particle, whereas the element type with reduced integration C3D8R was used for the composites. The data of the meshed nodes and elements for CNF nanopaper were generated by MATLAB subroutines, whereas the mesh for the GF/epoxy composite and the erodent particles were generated by TRUEGRID version 2.1.0. For all configurations, the mesh was refined near the impinging location to accurately capture the erosion.

Applied Polymer SCIENCE

**Table I.** Materials Constitutive Parameters Adopted in the Simulations

| Material | ρ (kg/m$^3$) | $E$ (GPa) | ν | $\sigma_y$ (GPa) | $E_p$ (GPa) | $\sigma_s$ (GPa) |
|---|---|---|---|---|---|---|
| $SiO_2$[21] | 2650 | 66.0 | 0.17 | | | |
| Epoxy[22] | 1200 | 3.05 | 0.33 | 0.06 | 2.44 | 0.07 |
| GF[23,24] | 2550 | 72.3 | 0.33 | 1.03 | 142 | 2.0 |
| CNF[23,25] | 1800 | 240 | 0.33 | 2.92 | 748 | 6.37 |

The $SiO_2$ was modeled using the linear elastic constitutive law, whereas epoxy, GF, and CNF were modeled using elastic-plastic constitutive law with linear isotropic hardening. The material parameters are listed in Table I,[21–25] where $\rho$ is the density, $E$ is the Young's modulus, $v$ is the Poisson's ratio, $\sigma_y$ is the yield stress, $E_p$ is the hardening modulus, and $\sigma_s$ is the material strength. The physical meanings of the parameters can be revealed by the stress $\sigma$ versus strain $\varepsilon$ relation for uniaxial stretch of small deformation as in eq. (1). The small final plastic strain at breakage indicates the brittle property of all these materials.

$$\varepsilon = \begin{cases} \frac{\sigma}{E}, & \sigma < \sigma_y \\ \frac{\sigma}{E} + \frac{\sigma - \sigma_y}{E_p}, & \sigma \geq \sigma_y \end{cases} \quad (1)$$

To model the erosion of the target materials, a criterion needs to be introduced for the element removal.[26] In this work, a simple criterion based on the equivalent stress was applied for the element removal as in eq. (2). The element was removed, once its equivalent stress $\bar{\sigma}$ reached the critical value that was the material strength $\sigma_s$ in this work. Here, $\sigma'$ is the deviatoric stress tensor. This criterion can be simply implemented by the shear failure option available in ABAQUS/EXPLICIT.

$$\bar{\sigma} = \sqrt{\frac{3}{2}\sigma' : \sigma'} = \sigma_S \quad (2)$$

## RESULTS AND DISCUSSION

Although both the nanopaper and the GF/epoxy composite showed brittle erosion behavior, that is, maximum erosion occurred at 90° impact angle, their erosion rate differed much in our experiments. To make the comparison more clearly, the GF/epoxy composite samples used for the erosion test was designed with half of the surface coated with nanopaper and half uncoated as shown in Figure 4(a). After uniformly exposed to particle stream impacting for a given time, the unprotected half was severely eroded, whereas the half that was protected with the CNF nanopaper coating did not show much erosion [see Figure 4(a)]. The protection effect of the nanopaper coating can be clearly seen in the roughness profile of the eroded surface shown in Figure 4(b). The surfaces before and after erosion were inspected by SEM. Figure 5(a,b) show the surface of GF/epoxy composite before and after the erosion, respectively. Figure 5(c,d) show the surface of CNF nanopaper-coated GF/epoxy composite before and after the erosion, respectively. As shown in Figure 5(b), many microcracks caused by the impact of erodent particles can be seen in the GFs, and many small fragments of fibers can also be seen on the erosion surface. This is consistent with what was reported in the literature.[10] The erosion consists of the removal of matrix materials in the resin-rich areas such that the exposed fibers are no longer bonded to the composite. Consequently, fibers could easily break into fragments, causing serious fiber removal during erosion. For the surface protected by the CNF nanopaper coating, the matrix and CNF debris were tightly bonded. Exposed segments of CNFs could hardly be seen after particle erosion as shown in Figure 5(d).

The mass loss results are compared in Figure 6 for GF/epoxy composites with and without CNF nanopaper protective coating. The mass loss was calculated according to the measured sample weights before and after the erosion test. The error bars represent the standard deviation in three repeated tests. The CNF nanopaper (2.5 wt %) coated composites showed much smaller erosion amount, only 6.1% (volume fraction) of that of GF/epoxy composites. The poor erosion resistance of GF/epoxy composites may be attributed to the inclusion of more brittle GFs (65 wt %). Another major difference is the interweaved structure of CNFs in the nanopaper, which might have provided a strong shielding effect to protect the relative weak resin matrix from impact loading.

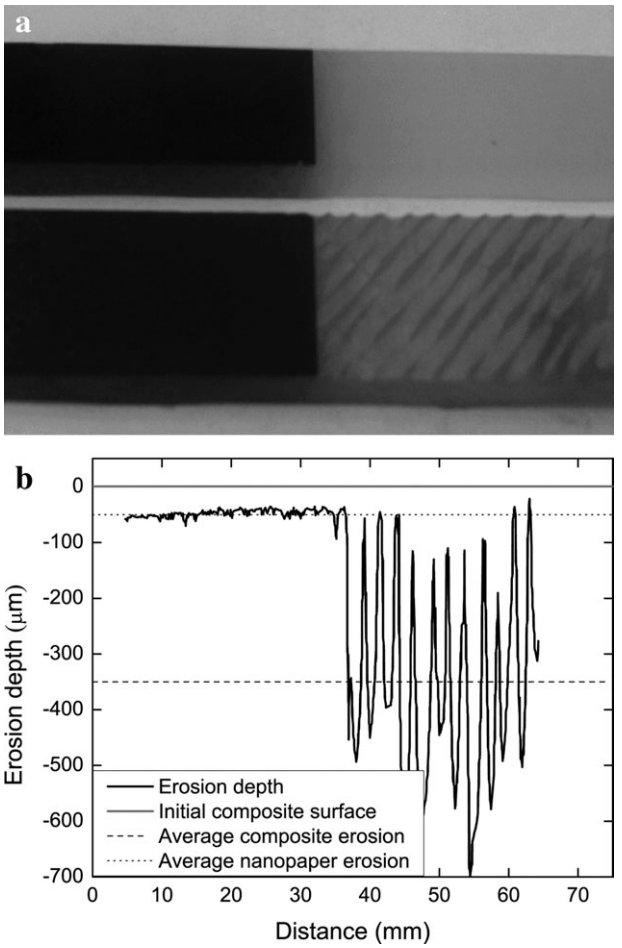


**Figure 4.** (a) Comparison of the uneroded and eroded surface morphology of GF/epoxy composites with and without CNF nanopaper coating and (b) surface profile of eroded samples.

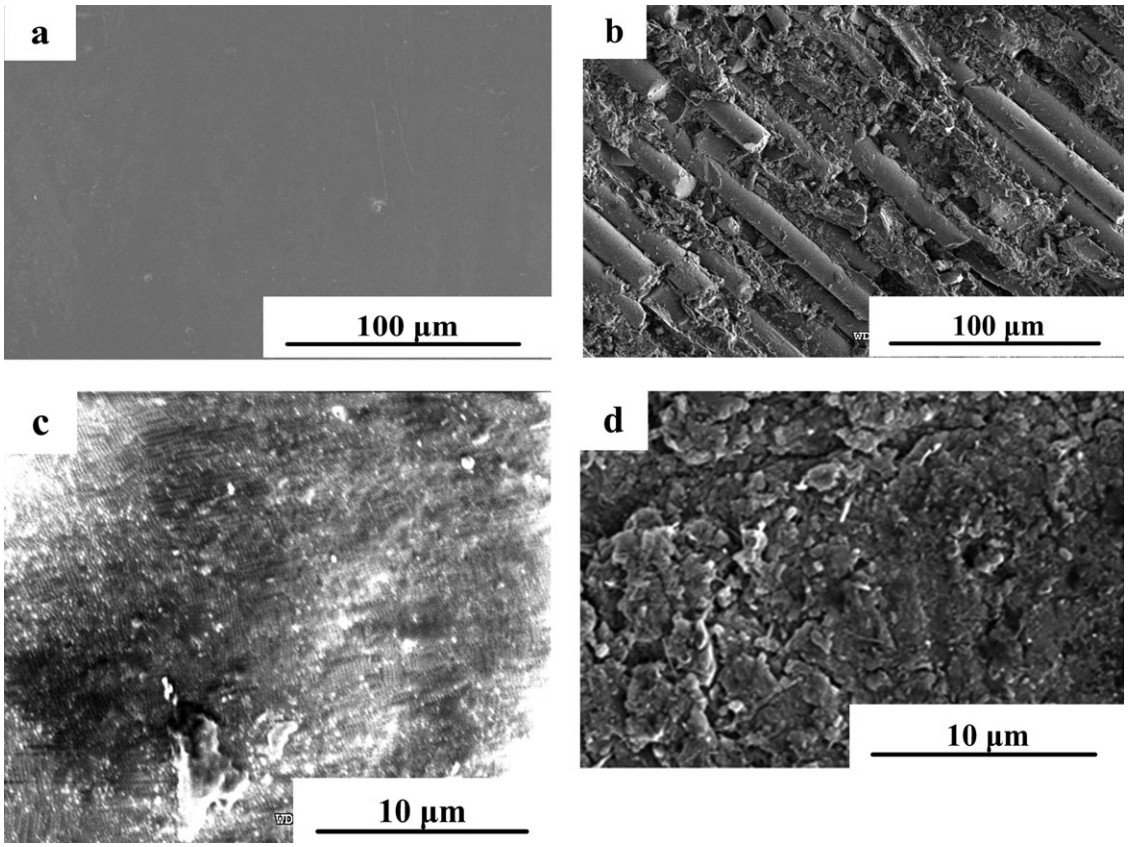


**Figure 5.** SEM images: (a) and (b) GF/epoxy composites before and after particle erosion, respectively; (c) and (d) CNF nanopaper before and after particle erosion, respectively.

The FE simulation results reproduced the experimentally observed differences. Figure 7 shows the simulated results of the effect of impinging positions on the eroded volume for GF/epoxy composite of 0.3-mm thick and nanopaper of 0.1-mm thick. Three representative positions A, B, and C were investigated for GF/epoxy composites, whereas two positions D and E were investigated for CNF nanopaper as indicated in Figure 7(b). Noting that for position C, a larger configuration containing one complete instead of a quarter of erodent was needed for the simulation RVE because of lacking symmetry. For that position, the degrees of freedom of the nodes on the opposite lateral faces of target were correspondingly coupled using the linear equations. The eroded volume was calculated as one-fourth of the amount in the simulation of the RVE. Using periodicity, one can plot the eroded volume versus the distance along the target surface in Figure 7(a). The results show that the erosion rate for GF/epoxy composites is much larger than that for CNF nanopaper, consistent with the experimental results in Figure 6. In addition, Figure 7(a) shows that the erosion rate is more sensitive to the impinge locations for GF/epoxy composites than for nanopaper. The much smoother profile of the eroded surface for CNF nanopaper can, therefore, be explained qualitatively. The fiber spacing in the GF/epoxy composite is larger or comparable to the particle size, and the resin between fibers cannot be effectively protected. While in the nanopaper the fiber spacing is much smaller, a large number of interconnected fibers come into contact with the erodent at the same time wherever the impinge location is, and the fibers can bear the impact force together.

Figure 8 shows the calculated eroded volume for GF/epoxy composites with and without CNF nanopaper coating for

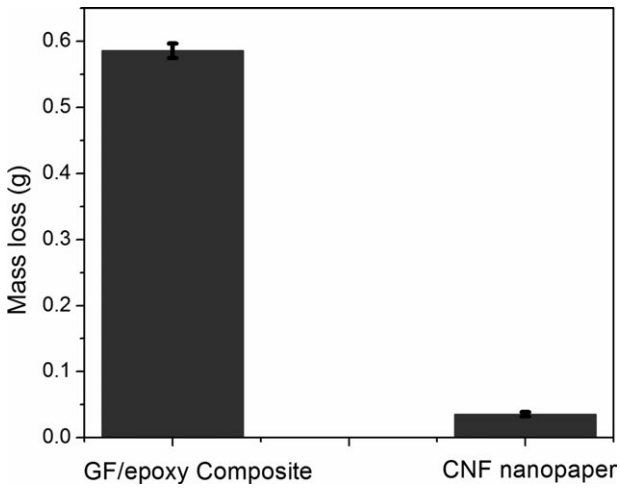


**Figure 6.** Mass loss of GF/epoxy composites with and without CNF nanopaper coating after 30 s of erosion at a distance of 7.6 cm from the spout and an impingement angle of 90°.

Applied Polymer SCIENCE

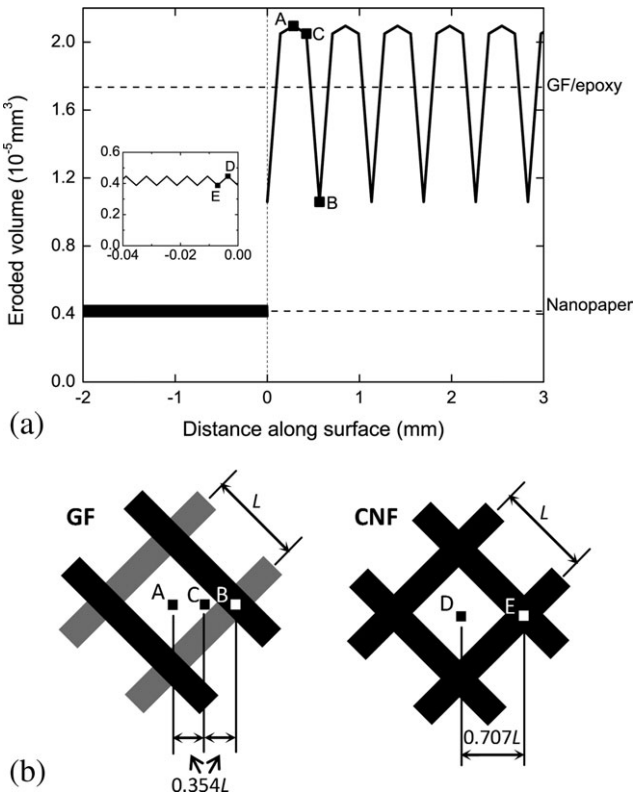


**Figure 7.** Comparison of the effect of impinging positions on the eroded volume for GF/epoxy composites and CNF nanopaper. (a) The eroded volume versus distance on the surface, with left curve for nanopaper and right for GF/epoxy and (b) vertical view of the different impinging positions, where *L* is the distance between fiber axes.

different sample thicknesses. The eroded volumes were averaged for different particle impinging positions as shown in Figure 7. The simulation results are in good qualitative agreement with the experimental data in Figure 6. The eroded volume did not change much with sample thickness, which is also consistent with our experimental observations (data not shown).

Using FE simulations, we also investigated the effects of CNF content in the nanopaper for particle erosion protection. As shown in Figure 9, a higher CNF content leads to better erosion resistance. This effect comes from the fact that the spacing between CNFs is smaller at a higher CNF content, and consequently more CNFs can partake the force of the impacting particle at the same time. The microstructure dimension, especially the fiber interspace plays an important role in the particle erosion resistance. When the fiber spacing is comparable to or even larger than the erodent size, the protection effect provided by the fibers becomes insignificant, as in the case of the conventional GF/epoxy composites. This investigation provides insights for the different particle erosion resistance between the nanopaper and the conventional GF/epoxy composites.

As CNF is relatively inexpensive and can form nanopaper easily, we focused this work on CNF-based nanopaper. On the other hand, our experimental and simulation analyses clearly show that smaller carbon nanoparticles with high aspect ratios, such

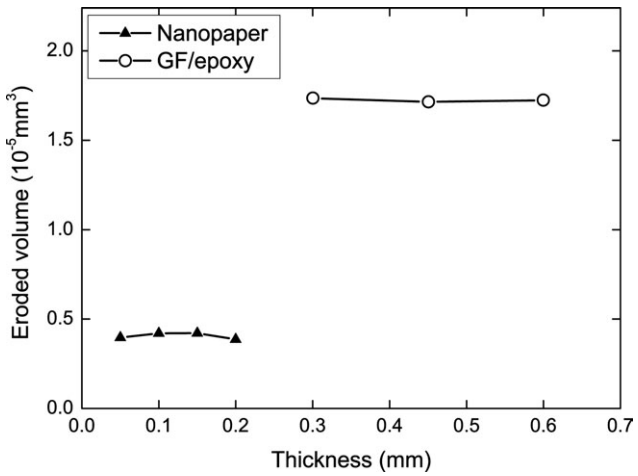


**Figure 8.** Simulation results of eroded volume versus thickness for GF/epoxy composites and CNF nanopaper.

as CNTs, should be able to provide better particle erosion protection due to the smaller tube interspace and higher mechanical properties of CNT-based nanopapers. However, it is more difficult to prepare nanopapers by CNT than by CNF, because the length of the CNT is much shorter than that of the CNF. For proof of the concept, we directly sprayed CNF and multiwall CNT (MWCNT) on the surface of the GF mats before making epoxy composites, and then carried out the same erosion-resistance test. Both CNF and MWCNT are 1% weight fraction of the GF. The results show much less mass loss in the MWCNT-based composite, 0.014 + 0.003 g than in the CNF-based composite, 0.078 ± 0.004 g when both samples were subject to 30 s particle erosion with the nozzle placed 7.6 cm away from the sample surface.

## CONCLUSIONS

The CNF nanopaper can achieve much better particle erosion resistance than the conventional GF/epoxy composites. The trends of the FE simulations agree well with the particle erosion

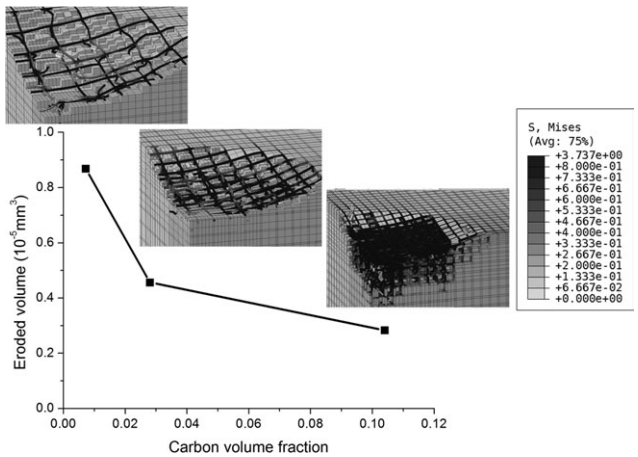


**Figure 9.** Eroded volume for nanopapers with different CNF contents. Snapshot plots the eroded configuration near impact position with von Mises stress contours.

experiments and provide insights regarding the underlying mechanisms. The excellent erosion resistance makes the CNF nanopaper a prospective protective coating material for turbine blades in wind energy industry, as well as for helicopter propeller blades.

## ACKNOWLEDGMENTS

Glass fiber mats were donated by Owens Corning (Toledo, OH), and wind epoxy was donated by Hexion, Columbus, OH. The first author Na Zhang acknowledges the China Scholarship Council for their financial support to enable the author to study at The Ohio State University.

## REFERENCES

1. http://www.nrgsystems.com/AboutWind/BenefitsofWindEnergy.aspx (accessed September 30, 2012).
2. Dalili, N.; Edrisy A.; Carriveau R. *Renew. Sust. Energy Rev.* **2009**, *13*, 428.
3. Tsiang, T. H. *J. Compos. Technol. Res.* **1986**, *8*, 154.
4. Pool, K. V.; Dharan, C. K. H.; Finnie, I. *Wear* **1986**, *107*, 1.
5. Tilly, G. P. *Wear* **1969**, *14*, 63.
6. Smeltzer, C. E.; Gulden, M. E.; Compton, W. A. *J. Basic Eng.* **1970**, *19*, 639.
7. Mallick, P. K. Fiber-Reinforced Composites: Materials, Manufacturing, and Design, 3rd ed.; CRC Press: Boca Raton, FL, **2007**.
8. Palmeri, M. J.; Putz, K. W.; Ramanathan, T.; Brinson, L. C. *Compos. Sci. Technol.* **2011**, *71*, 79.
9. Tewaria, U. S.; Harshaa, A. P.; Hagerb, A. M.; Friedrichb, K. *Compos. Sci. Technol.* **2003**, *63*, 549.
10. Patnaik, A.; Satapathy, A.; Chand, N.; Barkoulad, N. M.; Biswasb, S. *Wear* **2010**, *268*, 249.
11. Miyazaki, N.; Takeda, N. *J. Compos. Mater.* **1993**, *27*, 21.
12. Barkoula, N. M.; Karger-Kocsis, J. *J. Mater. Sci.* **2002**, *37*, 3807.
13. Cai, Z. Q.; Movva, S.; Chiou, N. R.; Guerra, D.; Hioe, Y.; Castro, J. M.; Lee, L. J. *J. Appl. Polym. Sci.* **2010**, *118*, 2328.
14. Zhou, G.; Movva, S.; Lee, L. *J. Polym. Compos.* **2009**, *30*, 861.
15. Balani, K.; Harimkar, S. P.; Keshri, A.; Chen, Y.; Dahotre, N. B.; Agarwal, A. *Acta Mater.* **2008**, *56*, 5984.
16. Bao, L.; Qian, D.; Wang, G.; Kemmochi, K. *J. Textile Eng.* **2012**, *58*, 13.
17. Liang, F.; Gou, J.; Kapat, J.; Gu, H.; Song, G. *Int. J. Smart Nano Mater.* **2011**, *2*, 120.
18. ElTobgy, M. S.; Ng, E.; Elbestawi, M. A. *Int. J. Mach. Tool Manuf.* **2005**, *45*, 1337.
19. Takaffoli, M.; Papini, M. *Wear* **2009**, *267*, 144.
20. Shimizu, K.; Noguchi, T.; Seitoh, H.; Okadab, M.; Matsubara, Y. *Wear* **2001**, *250*, 779.
21. Ei-Kareh, B. Fundamentals of Semiconductor Processing Technologies; Kluwer Academic Publishers: Norwell, MA, **1995**; pp 40–41.
22. Low, K. H.; Wang, Y. *Circuit World* **2007**, *33*, 9.
23. Grace, N. F.; Ragheb, W. F.; Sayed, G. A. *Compos. Struct.* **2004**, *64*, 521.
24. Agarwal, B. D.; Broutman, L. J.; Chandrashekhara, K. Analysis and Performance of Fiber Composites, 3rd ed.; Wiley: New York, **2006**, pp 8–9.
25. Tibbetts, G. G.; McHugh, J. J. *J. Mater. Res.* **1999**, *14*, 2871.
26. Wang, Y. F.; Yang, Z. G. *Wear* **2008**, *265*, 871.